Proceedings of the
2007 IEEE Intelligent Vehicles Symposium
Istanbul, Turkey, June 13-15, 2007

Enhancement of Handling and Cornering Capability for Individual Wheel Braking Actuated Vehicle Dynamics

Erkin Dinçmen and Tankut Acarman

Abstract— **In this paper, active safety enhancement for individual wheel braking actuated vehicle dynamics is presented. The nonlinear tire characteristics play an important role during manoeuvering tasks since tire forces may be saturated when the tire slip angle exceeds some a priori unknown slip value. Saturated forces, especially in the lateral direction, may result in an increase on the vehicle side slip angle and manoeuvering task may not be accomplished safely while the vehicle is drifting out of its trajectory. Regulation of tire forces may be very difficult at controller development stage due to modeling and analytical complexities and due to the presence of many unknown factors such as the road-tire friction coefficient. This paper proposes a controller methodology that may prevent the saturation of the lateral tire forces by regulating the individually actuated wheel brake actuators. The phenomenon of tire force saturation in the lateral direction is detected by comparing the individually estimated lateral tire force with its linear form simultaneously, and regulating the decentralized individual hydraulic wheel brakes to reduce the tire slip angles. Simulation results are illustrated to show the effectiveness of the proposed approach.**

I. INTRODUCTION

One of the main reasons of vehicle accidents is driver's inability to judge properly the limits of his/her vehicle. When the speed of the vehicle exceeds a safe speed limit with respect to the road curvature and the tire-road friction coefficient, the driver may loose control of the vehicle. Since accidents are mainly caused by the driver's control authority failure at sensing the vehicle limits and intervening before the possible hazards, driver assistance systems have been introduced to assure active safety. In [1], [2] and [3], using a reference vehicle model, the desired yaw rate has been calculated from the driver inputs. Regulating the differential braking or coordinating the active steering and individually actuated braking methods, the lateral stability of the vehicle model has been shown to be assured. During short-time emergency manoeuvering tasks, the driving physical limits depend primarily on the tire-road friction coefficient. The tire-road friction and consequently, tire forces in both of the lateral and the longitudinal direction may be estimated to accomplish safe manoeuvering tasks in the physical limits. In [4], the tire-road friction coefficient has been estimated by using a recursive least square identification algorithm during braking manoeuver.In [5], the tire forces by using an Extended Kalman Filter has been estimated and compared with a reference force, resulted by road friction coefficient estimation. Road friction coefficient estimation may be computationally complex on a real-time basis.

The second author would like to acknowledge support of the Turkish National Research Council TUBITAK under grant no: 106E121.

E. Dinçmen is with the Department of Mechanical Engineering, Istanbul Technical University, Inonu Cad., 87 Gumussuyu, TR-34437, Istanbul, Turkey. erkin.dincmen@itu.edu.tr

T. Acarman is with Faculty of Engineering and Technology, Computer Engineering Department, University of Galatasaray, Ciragan Cad., 36, Ortakoy, TR-34357, Istanbul, Turkey. tacarman@gsu.edu.tr

In this paper, safety is assured by comparing deviation of each individual tire force in the lateral direction from the linear characteristics, and then possible saturation effects are detected. Lateral tire forces are calculated based on the estimation of generated tire forces in the longitudinal direction during braking manoeuver. ABS control and extremum seeking is revisited in order to estimate tire forces in a finite time with high accuracy. And then the methodology is proposed to regulate the individually actuated hydraulic brake actuators and to operate in the stable region of the tire characteristics at the lower slip angle values generating the higher tire force output.

The remainder of this paper is organized as follows. In Section 2 the vehicle model, wheel dynamics and tire model is presented. Section 3 introduces the control algorithm and estimation of lateral forces. Simulation results are given in Section 4. Finally, some results are given to conclude the paper.

II. MODELLING

A. Vehicle Model

A nonlinear double track vehicle model with nonlinear tire characteristics is considered towards controller design. The equations of motion dynamics are given by,

$$\dot{u} = \frac{Fx_{sum}}{m} + vr - \frac{1}{2}A_\rho |u| u \tag{1}$$

$$\dot{v} = \frac{Fy_{sum}}{m} - ur \tag{2}$$

$$\dot{r} = \frac{Mz_{sum}}{I_z} \tag{3}$$

where m denotes the vehicle mass, A_ρ the aerodynamic drag force coefficient, I_z is the yaw inertia, r is the yaw rate, u and v denotes velocities in the longitudinal and lateral direction, respectively, as illustrated in Fig.1. Fx_{sum}, Fy_{sum} and Mz_{sum} are the sum of forces and moment acting on the vehicle model

$$\begin{aligned} Fx_{sum} &= (Fx_1 + Fx_2)\cos\delta_f - (Fy_1 + Fy_2)\sin\delta_f \\ &\quad + Fx_3 + Fx_4 \\ Fy_{sum} &= (Fx_1 + Fx_2)\sin\delta_f + (Fy_1 + Fy_2)\cos\delta_f \\ &\quad + Fy_3 + Fy_4 \end{aligned}$$

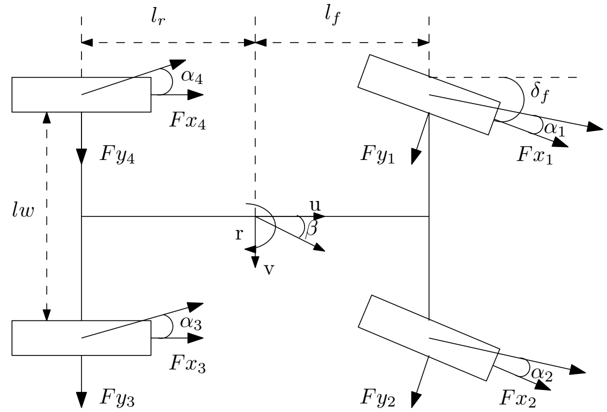

Fig. 1. Top view of the vehicle model

$$\begin{aligned}Mz_{sum} &= ((Fx_1 - Fx_2)\cos\delta_f - (Fy_1 - Fy_2)\sin\delta_f)\frac{lw}{2} \\ &+ ((Fx_1 + Fx_2)\sin\delta_f + (Fy_1 + Fy_2)\cos\delta_f)l_f \\ &+ (Fx_4 - Fx_3)\frac{lw}{2} - (Fy_3 + Fy_4)l_r\end{aligned}$$

Here δ_f is the front wheel steering angle, l_f and l_r are the distances from center of gravity (CG) to the front and rear axle, lw denotes the front and rear track width. The tire slip angles are calculated as follows:

$$\alpha_1 = \delta_f - \tan^{-1}\left(\frac{v + rl_f}{u + rlw/2}\right) \tag{4}$$

$$\alpha_2 = \delta_f - \tan^{-1}\left(\frac{v + rl_f}{u - rlw/2}\right) \tag{5}$$

$$\alpha_3 = -\tan^{-1}\left(\frac{v - rl_r}{u - rlw/2}\right) \tag{6}$$

$$\alpha_4 = -\tan^{-1}\left(\frac{v - rl_r}{u + r \cdot lw/2}\right) \tag{7}$$

B. Wheel Dynamics

Rotational motion dynamics for each individual tire, *i.e.*, for $i = 1, 2, 3, 4$, are given by,

$$\dot{\omega}_i = \frac{T_d - T_{bi} - RF_{xi} - dF_{zi}}{I_w} \tag{8}$$

where ω_i denotes the $i - th$ tire angular velocity, T_d is traction moment, T_{bi} is individual wheel braking moment, F_{zi} is tire vertical force, I_w denotes the wheel inertia, R is the tire effective radius and d is the vertical tire force offset as illustrated in Fig.2. For simplicity, the dynamic weight transfer is neglected and the vertical tire forces are given by,

$$Fz_1 = Fz_2 = \frac{mg}{2}\frac{l_r}{l_f + l_r} \tag{9}$$

$$Fz_3 = Fz_4 = \frac{mg}{2}\frac{l_f}{l_f + l_r} \tag{10}$$

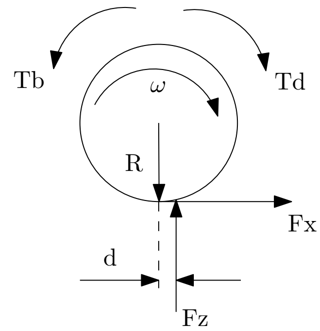

Fig. 2. Forces and moments acting on the wheel model

C. Tire Forces

Modelling tire forces along the longitudinal and lateral axes, Dugoff's tire model is used. Towards controller derivation and analysis, Dugoff's model presents significant advantage of being analytical where an alternative tire model introduced Pacejka and Sharp is semi-empirical, [9].

Dugoff's model may be analytically derived at controller's development stage. Combined longitudinal and lateral force generation are directly related to the tire road coefficient in compact form,

$$F_{xi} = C_{xi}\frac{\kappa_i}{1 + \kappa_i}f(\lambda_i) \tag{11}$$

$$Fy_i = Cy_i\frac{\tan(\alpha_i)}{1 + \kappa_i}f_i(\lambda_i) \tag{12}$$

where Cx_i and Cy_i are the $i - th$ tire longitudinal and lateral cornering stiffness, respectively. The variable λ_i and the function $f_i(\lambda_i)$ are given,

$$\lambda_i = \frac{\mu Fz_i(1 + \kappa_i)}{2\sqrt{(Cx_i\kappa_i)^2 + (Cy_i\tan(\alpha_i))^2}} \tag{13}$$

$$f_i(\lambda_i) = \begin{cases}(2 - \lambda_i)\lambda_i & \text{if } \lambda_i < 1 \\ 1 & \text{if } \lambda_i \geq 1\end{cases} \tag{14}$$

where μ denotes the tire-road friction coefficient. The tire slip ratios during braking are given by,

$$\kappa_i = -\frac{u_{ti} - R\omega_i}{u_{ti}} \tag{15}$$

where u_{ti} is the velocity on rolling direction for $i - th$ individual tire given by,

$$\begin{aligned}u_{t1} &= (u + r(lw/2))\cos\delta_f + (v + rl_f)\sin\delta_f \\ u_{t2} &= (u - r(lw/2))\cos\delta_f + (v + rl_f)\sin\delta_f \\ u_{t3} &= (u - r(lw/2)) \\ u_{t4} &= (u + r(lw/2))\end{aligned} \tag{16}$$

III. CONTROL ALGORITHM

The proposed controller is built on the observation of the deviation between the individual nonlinear tire force and the linear characteristics. The main purpose of this approach is to enforce the tire forces stay in the linear region and to generate high tire force with respect to tire slip angle

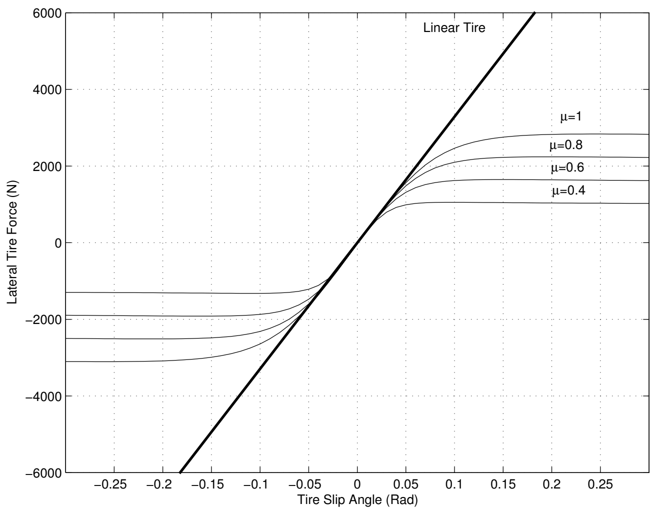

Fig. 3. Lateral tire force characteristics.

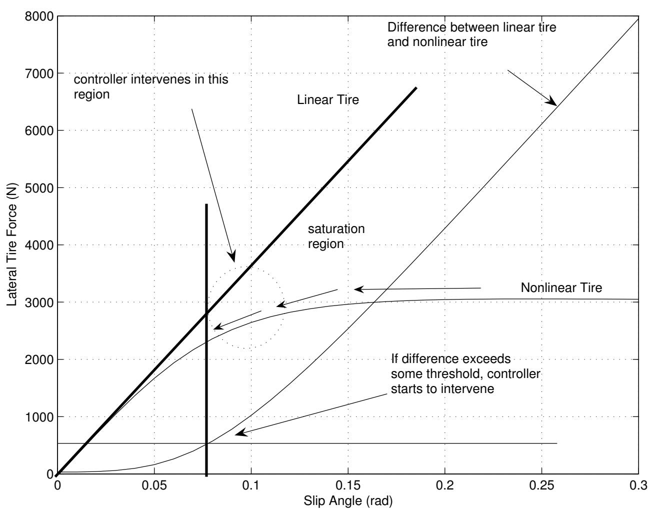

Fig. 4. Individual braking operation region to prevent tire force saturation.

improving cornering and handling capability of the vehicle motion. Even though the tire forces are entered into the saturation region, so-called "$unstable\ region$", where tire forces outputs decrease while diverging with respect to the increasing tire slip angle, the proposed controller intervenes to this undesired transient operation by applying the required individual wheel braking that may enforce tire forces towards to the linear region. The nonlinear tire force characteristics are plotted in Fig.3 for different road friction coefficients where the proposed methodology is illustrated in Fig.4.

The estimation of front axle and rear axle lateral tire forces is based on longitudinal tire force estimation, lateral acceleration and yaw rate measurement, [8]. Estimation of tire longitudinal force is based on tire angular velocity measurement, [7]. The simplified longitudinal tire dynamics may be given by,

$$I_w \dot{\omega}_i = T_d - T_{bi} - RF_{xi} \tag{17}$$

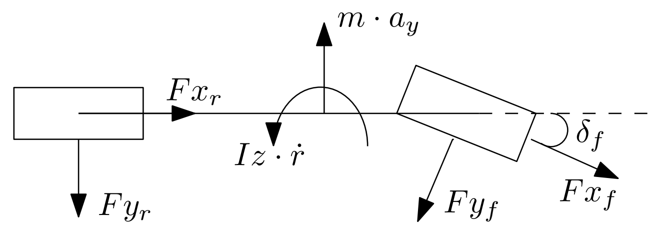

Fig. 5. Forces and moments acting on a single track vehicle model

The rolling resistance effect hasn't been taken into consideration at observer design stage. Defining the variable $\hat{\omega}_i$,

$$I_w \dot{\hat{\omega}}_i = T_d - T_{bi} + RM\text{sign}(\bar{\omega}_i) \tag{18}$$

where $\bar{\omega}_i = \omega_i - \hat{\omega}_i$ is the error between the estimated and the measured tire angular velocity. Subtracting (18) from (17),

$$I_w \dot{\bar{\omega}}_i = -M\text{sign}(\bar{\omega}_i)R - RF_{xi} \tag{19}$$

By choosing $|M| > \max|F_x|$, the estimated state, $\hat{\omega}_i$ may track the real state, ω_i, due to discontinuous feedback in the observer equation. In sliding mode, the equivalent value of $M\text{sign}(\bar{\omega}_i)$ is equal to the longitudinal tire force,

$$\hat{F}x_i = -\left(M\text{sign}(\bar{\omega}_i)\right)_{eq} \tag{20}$$

To obtain the equivalent value of $M\text{sign}(\bar{\omega}_i)$ during sliding mode, a low pass filter is used. Hence, the equation of the filter is given by, (see also [7]),

$$\hat{F}x_i = -\left(1 - e^{-\frac{t}{\tau}}\right) M\text{sign}(\bar{\omega}_i) \tag{21}$$

where τ is the time constant of the filter to be chosen to attenuate the high frequency components in the original signal.

Force and moment acting on a single track vehicle model are illustrated in Fig.5. Equalizing moments to the rear and front axles, respectively, lateral tire force may be estimated,

$$\hat{F}y_f = \frac{1}{\cos\delta_f}\left(\frac{ma_y l_r + Iz\dot{r}}{l_f + l_r} - \hat{F}x_f \sin\delta_f\right) \tag{22}$$

$$\hat{F}y_r = \frac{ma_y l_f - Iz\dot{r}}{l_f + l_r} \tag{23}$$

where $\hat{F}y_f$ and $\hat{F}y_r$ are the estimation of front and rear axle total lateral force and a_y is the lateral acceleration. $\hat{F}x_f$ is estimated front axle total longitudinal force and it is calculated as follows:

$$\hat{F}x_f = \hat{F}x_1 + \hat{F}x_2 \tag{24}$$

A. Nonlinear Controller Development Based on the Individual Wheel Braking Actuated Vehicle Model

The error between the nonlinear front axle lateral force and its linearized value is written as follows:

$$\begin{aligned} e_f &= Fy_{flin} - Fy_f \qquad (25) \\ &= Cy_f\alpha_f - Cy_1\frac{\tan\alpha_1}{1+\kappa_1}f_1(\lambda_1) - Cy_2\frac{\tan\alpha_2}{1+\kappa_2}f_2(\lambda_2) \end{aligned}$$

where Fy_f is front axle total lateral force, Fy_{flin} denotes the linearized value, Cy_f is the front axle total cornering stiffness and α_f is the front axle slip angle given by,

$$\alpha_f = \delta_f - \beta - \frac{l_f r}{u} \tag{26}$$

The time-derivative of the error, given by (25), subjected to the front axle in the lateral direction may be derived,

$$\begin{aligned}\dot{e}_f =& Cy_f\dot{\alpha}_f - Cy_1\frac{\dot{\alpha}_1(1+\kappa_1)}{\cos^2\alpha_1(1+\kappa_1)^2}f_1(\lambda_1) \\ &- Cy_2\frac{\dot{\alpha}_2(1+\kappa_2)}{\cos^2\alpha_2(1+\kappa_2)^2}f_2(\lambda_2) \\ &+ Cy_1\frac{\tan\alpha_1}{(1+\kappa_1)^2}f_1(\lambda_1)\dot{\kappa}_1 + Cy_2\frac{\tan\alpha_2}{(1+\kappa_2)^2}f_2(\lambda_2)\dot{\kappa}_2 \\ &- Cy_1\frac{\tan\alpha_1}{1+\kappa_1}\frac{\partial f_1}{\partial\lambda_1}\dot{\lambda}_1 - Cy_2\frac{\tan\alpha_2}{1+\kappa_2}\frac{\partial f_2}{\partial\lambda_2}\dot{\lambda}_2\end{aligned} \tag{27}$$

Deriving $\dot{\kappa}_i$ in terms of the wheel states and reconsidering the tire dynamics given in (8) during braking, for i=1,2,3,4,

$$\dot{\omega}_i = \frac{-Tb_i - R\hat{F}x_i}{I_w} \tag{28}$$

$$\dot{\kappa}_i = -(\kappa_i+1)\frac{\dot{u}_{ti}}{u_{ti}} - \frac{R^2}{I_w}\frac{\hat{F}_{xi}}{u_{ti}} - \frac{R}{I_w}\frac{1}{u_{ti}}T_{bi} \tag{29}$$

The time-derivative (27) may be rewritten,

$$\begin{aligned}\dot{e}_f =& Cy_f\dot{\alpha}_f - Cy_1\frac{\dot{\alpha}_1}{\cos^2\alpha_1(1+\kappa_1)}f_1(\lambda_1) \\ &- Cy_1\frac{\tan\alpha_1}{1+\kappa_1}\frac{\partial f_1}{\partial\lambda_1}\dot{\lambda}_1 - \left(Cy_1\frac{\tan\alpha_1}{(1+\kappa_1)^2}f_1(\lambda_1)\right) \\ &\cdot\left((\kappa_1+1)\frac{\dot{u}_{t1}}{u_{t1}} + \frac{R^2}{I_w}\frac{\hat{F}_{x1}}{u_{t1}} + \frac{R}{I_w}\frac{1}{u_{t1}}T_{b1}\right) \\ &- Cy_2\frac{\dot{\alpha}_2}{\cos^2\alpha_2(1+\kappa_2)}f_2(\lambda_2) \\ &- Cy_2\frac{\tan\alpha_2}{1+\kappa_2}\frac{\partial f_2}{\partial\lambda_2}\dot{\lambda}_2 - \left(Cy_2\frac{\tan\alpha_2}{(1+\kappa_2)^2}f_2(\lambda_2)\right) \\ &\cdot\left((\kappa_2+1)\frac{\dot{u}_{t2}}{u_{t2}} + \frac{R^2}{I_w}\frac{\hat{F}_{x2}}{u_{t2}} + \frac{R}{I_w}\frac{1}{u_{t2}}T_{b2}\right)\end{aligned} \tag{30}$$

Modelling the vehicle dynamics, the tire velocities on rolling directions are calculated in (16). At controller design stage, the following equations denote the time-derivative of tire velocities on the rolling direction,

$$\begin{aligned}\dot{u}_{t1} &= \dot{u} + \dot{r}(lw/2) \\ \dot{u}_{t2} &= \dot{u} - \dot{r}(lw/2) \\ \dot{u}_{t3} &= \dot{u} - \dot{r}(lw/2) \\ \dot{u}_{t4} &= \dot{u} + \dot{r}(lw/2)\end{aligned} \tag{31}$$

Time derivative of the longitudinal velocity is calculated in (1). Here, it is simplified with neglecting aerodynamic drag force and under small angle assumptions,

$$\dot{u} = \frac{\hat{F}x_{total} - \hat{F}y_f\delta_f}{m} + vr \tag{32}$$

where

$$\hat{F}x_{total} = \hat{F}x_1 + \hat{F}x_2 + \hat{F}x_3 + \hat{F}x_4 \tag{33}$$

Through straight forward manipulations, the individual braking torque applied to the front tires are chosen such that $e_f \to 0$ and $\dot{e}_f \to 0$ are satisfied outside the region Δ as $t \to \infty$,

$$\begin{aligned}Tb_1 = \Bigg[&\frac{I_w(1+\kappa_1)}{R}\left(-\frac{\hat{F}x_{total}}{m} + \frac{\hat{F}y_f}{m}\delta_f - vr - \dot{r}\frac{l_w}{2}\right) \\ &- R\hat{F}_{x1} + \frac{I_w u_{t1}}{R} \\ &\cdot\left(k_{11}|\dot{\alpha}_f| + k_{12}|\dot{\alpha}_1| + M_1\right)sign(tan(\alpha_1))\Bigg]\Gamma_{sign}(e_f)\end{aligned} \tag{34}$$

$$\begin{aligned}Tb_2 = \Bigg[&\frac{I_w(1+\kappa_2)}{R}\left(-\frac{\hat{F}x_{total}}{m} + \frac{\hat{F}y_f}{m}\delta_f - vr + \dot{r}\frac{l_w}{2}\right) \\ &- R\hat{F}_{x2} + \frac{I_w u_{t2}}{R} \\ &\cdot\left(k_{21}|\dot{\alpha}_f| + k_{22}|\dot{\alpha}_2| + M_2\right)sign(tan(\alpha_2))\Bigg]\Gamma_{sign}(e_f)\end{aligned} \tag{35}$$

Without loosing of generality, the controller derived to regulate lateral deviation subjected to the front axle may be repeated for the rear axle, defining,

$$\dot{e}_r = \dot{F}y_{rlin} - \dot{F}y_r \tag{36}$$

where Fy_{rlin} is rear axle linearized total lateral force,

$$Fy_{rlin} = Cy_r\alpha_r \tag{37}$$

where Cy_r is the rear axle total cornering stiffness, α_r is the rear axle slip angle given by,

$$\alpha_r = -\beta + \frac{l_r r}{u} \tag{38}$$

To stabilize lateral deviation subjected to the rear axle, the controller's outputs are derived by,

$$\begin{aligned}Tb_3 = \Bigg[&\frac{I_w(1+\kappa_3)}{R}\left(-\frac{\hat{F}x_{total}}{m} + \frac{\hat{F}y_f}{m}\delta_f - vr + \dot{r}\frac{l_w}{2}\right) \\ &- R\hat{F}_{x3} + \frac{I_w u_{t3}}{R} \\ &\cdot\left(k_{31}|\dot{\alpha}_f| + k_{32}|\dot{\alpha}_3| + M_3\right)sign(tan(\alpha_3))\Bigg]\Gamma_{sign}(e_r)\end{aligned} \tag{39}$$

$$\begin{aligned}Tb_4 = \Bigg[&\frac{I_w(1+\kappa_4)}{R}\left(-\frac{\hat{F}x_{total}}{m} + \frac{\hat{F}y_f}{m}\delta_f - vr - \dot{r}\frac{l_w}{2}\right) \\ &- R\hat{F}_{x4} + \frac{I_w u_{t4}}{R} \\ &\cdot\left(k_{41}|\dot{\alpha}_f| + k_{42}|\dot{\alpha}_4| + M_4\right)sign(tan(\alpha_4))\Bigg]\Gamma_{sign}(e_r)\end{aligned} \tag{40}$$

where the gains k_{i1}, k_{i2} and M_i are chosen to be positive constants to satisfy $e_f \to 0$ and $\dot{e}_f \to 0$ outside the region Δ as $t \to \infty$. Also the discontinuous function $\Gamma_{sign}(\cdot)$

is a function with deadzone, (see Fig.6), assuring the time responses of the error between the linear and nonlinear forces to stay bounded, as illustrated in in Fig.4. Also, the terms $sign(tan(\alpha_i))$ satisfy that the control inputs to be always positive for both of the signs of the lateral forces, F_{yi}, for $i = 1, 2, 3, 4$. When the lateral force changes its sign, see for instance (12), i.e., they take negative values, the multiplicative term in the input term $sign(tan(\alpha_i))$ satisfy its positiveness. And the derived control inputs act on the wheel dynamics after being multiplied by "-1" as given in (28). Inside the region Δ, when the nonlinear tire force is increasing linearly with respect to tire slip angle, the individual brake torque, $i.e.$ controller output, is equal to zero.

Stability may be proven based on Lyapunov analysis through straigh forward manipulations and omitted due to space limit.

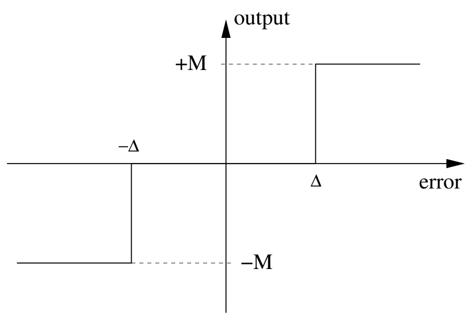

Fig. 6. Discontinuous function with deadzone.

IV. SIMULATION STUDIES

In this section, the performance of the proposed control algorithm is investigated through simulation studies. It is shown that the controller improves the vehicle's cornering capability considerably even on low road friction coefficients. During all scenarios, the deadzone in the discontinuous functions $\Gamma_{sign}(e_f)$ and $\Gamma_{sign}(e_r)$ are chosen to be same constant value, $\Delta = 200N$. These constants denote the braking operation point from which the nonlinear tire force saturates. The nonlinear Magic Formula tire model is performed with the numerical values given in [6] whereas the other vehicle model parameters belong to sedan type vehicle model. In the simulation scenarios, initially the vehicle model is traveling in a straight line with 20 m/s speed. The driver steering input is simulating an obstacle avoidance manoeuver, it is plotted in Fig.7. Simulations are performed by using the tire-road friction coefficient $\mu = 0.5$. The time-responses of the vehicle side slip angle β are plotted in Fig.8 for controlled and uncontrolled cases. It is shown that in the controlled case, the time responses of the side slip angle are more stable compared to the uncontrolled case assuring an improved cornering capability. In Fig.9 the yaw rate responses are plotted for both of the controlled and the uncontrolled cases compared with the generated desired yaw rate. Driver's desired yaw rate is calculated by

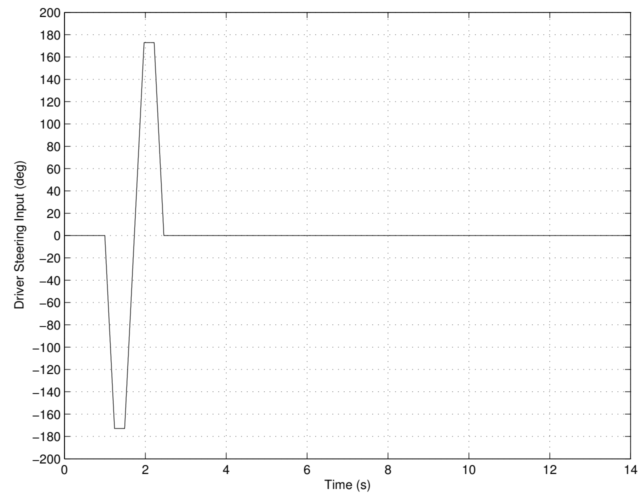

Fig. 7. The steering input

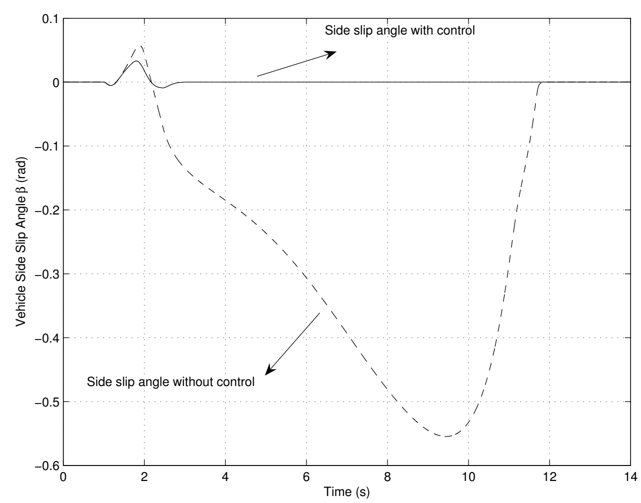

Fig. 8. The vehicle side slip angle for controlled (solid) and uncontrolled (dashed) scenarios.

using the driver's steering input and vehicle speed in the longitudinal direction as follows, [3]: $r_{des} = \frac{u\delta_f}{l_f + l_r + K_u u^2}$, where $K_u = m(l_r Cy_r - l_f Cy_f)/((l_f + l_r)Cy_f Cy_r)$. It is shown from Fig.9 that the controlled vehicle model can follow the desired yaw rate while the uncontrolled vehicle can not follow closely. In Fig.10, the vehicle model trajectories are plotted for controlled and uncontrolled cases. While the vehicle is skidding dangerously without control, with the proposed control algorithm, the vehicle model trajectories may follow the requested manoeuvering task. In Fig.11, the time responses of the longitudinal velocity are plotted. The uncontrolled velocity decreases considerably due to the dangerous skidding motion ended by heading instability. The controlled velocity in the longitudinal direction decreases due to the correcting individually actuated wheel braking effects, whose time responses are plotted in Fig.12.

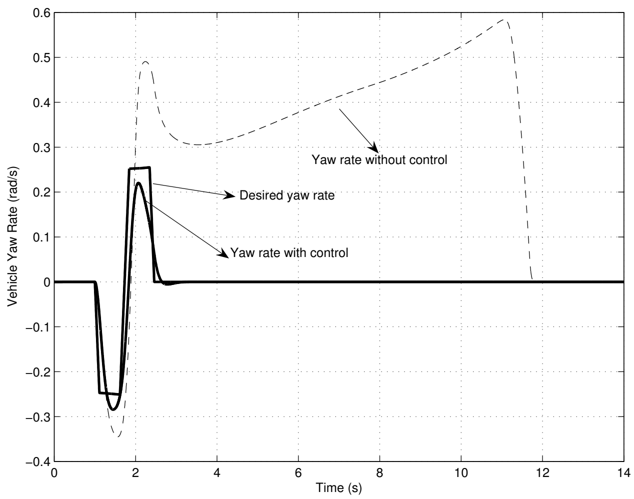

Fig. 9. The yaw rate for controlled (solid) and uncontrolled (dashed) scenarios.

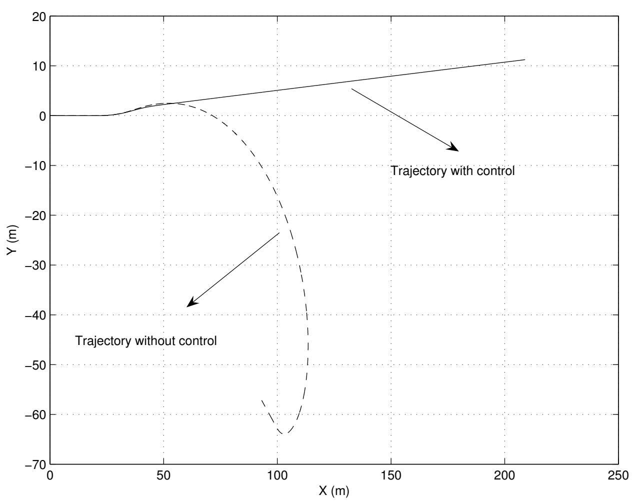

Fig. 10. The trajectories for controlled (solid) and uncontrolled (dashed) scenarios.

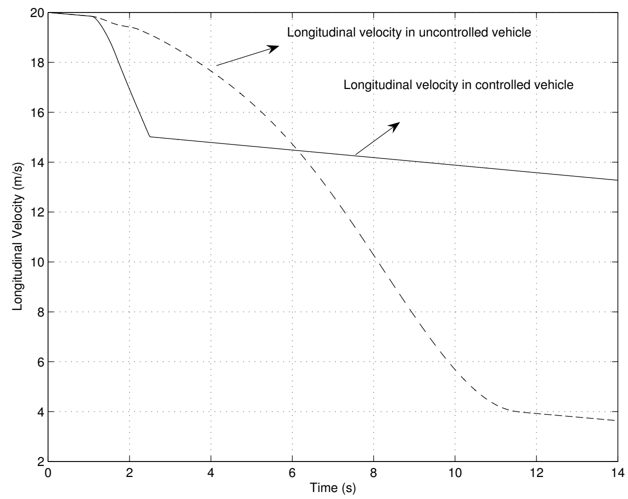

Fig. 11. The longitudinal velocity for controlled (solid) and uncontrolled (dashed) scenarios.

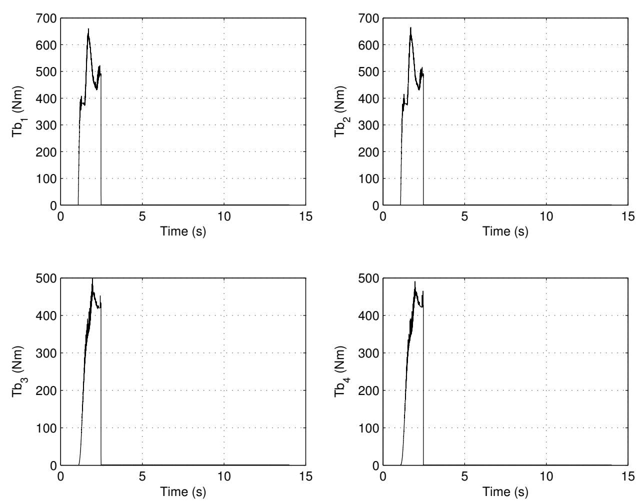

Fig. 12. The individual wheel braking inputs: T_{b1}, T_{b2}, T_{b3}, and T_{b4}.

V. CONCLUSIONS

In this study, a control algorithm improving vehicle cornering capability is introduced. Simulation scenarios are performed to validate the effectiveness of the proposed controller. The algorithm prevents lateral tire force saturation and keeps vehicle on the desired trajectory. Detecting the possibility of lateral tire force saturation through observing estimated lateral tire forces and their linearized values, the controller reduces the tire slip angles through regulating the individually actuated braking actuators to prevent saturation of lateral tire forces.

VI. ACKNOWLEDGMENTS

The authors gratefully acknowledge support of the European Union Framework Programme 6 through the AUTOCOM SSA project (INCO Project No: 16426) and The Scientific&Technological Research Council of Turkey (TUBITAK) in this paper.

REFERENCES

[1] E.Dinçmen, and T.Acarman, “Application of Vehicle Dynamics’ Active Control to a Realistic Vehicle Model ”, *accepted for publication in Proc. American Control Conference 2007*.
[2] A.T. van Zanten, R. Erhardt, and G. Pfaff, “VDC, The Vehicle Dynamics Control System of Bosch”, *SAE Technical Paper No:950759*, 1995.
[3] S. Zheng, H. Tang, Z. Han, Y. Zhang, “Controller Design for Vehicle Stability Enhancement”, *Control Engineering Practice*, vol. 14(12), 2006, pp.1413-1421.
[4] J. Wang, L. Alexander, R. Rajamani, “Friction Estimation on Highway Vehicles Using Longitudinal Measurements”, *Journal of Dynamic Systems, Measurement and Control*, vol. 126(2), 2004, pp.265-275.
[5] L. Ray, “Nonlinear Tire Force Estimation and Road Friction Identification: Simulation and Experiments”, *Automatica*, vol.33(10), 1997, pp. 1819-1833.
[6] H.B. Pacejka, *Tyre and Vehicle Dynamics*, Oxford:Butterworth-Heinemann, 2002.
[7] S. Drakunov, U. Ozguner, P. Dix, and B. Ashrafi, “ABS Control Using Optimum Search via Sliding Modes”, *IEEE Transc. on Control Systems Technology*, vol. 3(1), 1995, pp.79-85.
[8] Y. Fukada, “Slip Angle Estimation for Vehicle Stability Control”, *Vehicle System Dynamics*, vol. 32, 1999, pp.375-388.
[9] R. Rajamani, *Vehicle Dynamics and Control* , Springer, 2006.